Nanoscale

ARTICLE

Lanthanide Yb/Er Co-Doped Semiconductor Layered WSe_2 Nanosheets with Near-Infrared Luminescence in Telecommunication Wavelength

Received 00th January 20xx,
Accepted 00th January 20xx

DOI: 10.1039/x0xx00000x

www.rsc.org/

Gongxun Bai, Zhibin Yang, Huihong Lin, Wenjing Jie, Jianhua Hao*

Atomically thin layers of transition metal dichalcogenides (TMDs) have recently drawn great attention. However, doping strategies and controlled synthesis for wafer-scale TMDs are still in their early stages, greatly hindering constructing devices and further basic studies. In this work, we develop fast deposition of wafer-scale layered lanthanide ions Yb/Er co-doped WSe_2 by pulsed laser deposition. WSe_2 nanosheets are chosen as host, while Yb^{3+} and Er^{3+} ions serve as sensitizer and activator, respectively. The obtained Yb/Er co-doped WSe_2 layers exhibit good uniformity, high crystallinity with highly textured feature. Under the excitation of a diode laser at 980 nm, the down-conversion emission is observed at around 1540 nm, assigned to the emission transition between $^4I_{13/2}$ and $^4I_{15/2}$ states of Er^{3+}. Considering the significance of 1540 nm luminescence in application of photonic technologies, this observation in the WSe_2:Yb/Er nanosheets down to monolayer provides a new opportunity in conceiving photonic devices at 2D limit. Our works not only offer a general method to prepare wafer-scale lanthanide doped TMDs, but also widely modulate the luminescence of atomically layered TMDs through introducing lanthanide ions.

Introduction

Lanthanide ions usually doped in conventional insulators or semiconductor substrates as luminescent ions have abundant excited energy levels, allowing them to absorb and emit photons from ultraviolet (UV) to infrared regions.[1] Besides La^{3+} being similiar with Xe in electronic configuration, the lanthanide ions characterized by a partly filled 4f shell are shielded from their surroundings by the filled outer orbitals, producing a weak electron-phonon coupling and leading to narrow and sharp emission lines of inner 4f-4f transitions.[2] The luminescence of lanthanide activated ions shows the advantages of narrow bandwidth, high quantum yield, long lifetime and high light stability.[3] Nowadays, lanthanide ions activated luminescent materials have been widely used in photonic science and technology, covering many aspects.[4,5] In particular, lanthanide ions that can emit near-infrared (NIR) photons have been widely studied and applied in the fields of optoelectronic devices, optical fiber communication, and biomedicine.[6,7] Most importantly, the characteristic emission of Er^{3+} ions at 1.54 μm meets well with the minimum attenuation of silica optical fibers typically utilized in optical fiber communication.

On the other hand, as size of electronic and optoelectronic devices is progressively approaching the limits of conventional semiconductor technology,[8] due to short channel effects,[9] some new challenges must be addressed to fulfil these demands. Owing to the atomic scale thickness, one of the family of two-dimensional (2D) layered semiconductors, typically known as the transition metal dichalcogenides (TMDs) [10,11] e.g., WSe_2 and MoS_2 represent one such alternative that have drawn a great deal of interests for electronics and optoelectronics applications thanks to their excellent physical properties,[12,13] including good thermal stability, excellent mechanical strength, and high electrical conductivity, etc.[14] Due to the widening bandgap compared with graphene, layered TMDs semiconductors exhibit large exciton binding energies and flexibility, which have shown a great potential for next-generation optoelectronic devices,[15] such as solar cells, displays, optical sensor, and light-emitting diodes (LEDs).[16,17] However, both photoluminescence (PL) and electroluminescence of 2D layered semiconductors and devices are mainly confined in the spectral range from visible to NIR edges. The modulation of light is primarily performed by the bandgaps, excitons, and layer number. Noticeably, extending the luminescence of 2D layers to a wide range of NIR region, such as telecommunication around 1.54 μm, should be a significant milestone for both the basic research and application of the TMDs semiconductors. In general, chemical doping can greatly modulate the inherent properties of materials. Numerous doping approaches have been demonstrated for adjusting novel electronic materials (carbon nanotubes, graphene, organic semiconductors, etc.), and to

Department of Applied Physics, The Hong Kong Polytechnic University, Hong Kong, P. R. China
*Address correspondence to jh.hao@polyu.edu.hk

date some doping methods have also been utilized for tuning the luminescence in TMDs.[18,19] However, doping transition metal ions can only slightly shift the luminescent peaks in the previously reported metal ions doped TMDs.[20,21] Hence, it is essential to find a more effective approach to modulate the luminescence of TMDs.

At present, the study of TMDs mainly focuses on 2D disulfide semiconductors (MoS_2, WS_2, etc.) or diselenide semiconductors ($MoSe_2$, WSe_2, etc.), due to their interesting physical properties,[22] easy fabrication, and high thermal and chemical stability.[23] Recently, we have demonstrated that lanthanide Er^{3+} can be doped into the lattice of bi-layered MoS_2 by multiple steps of chemical synthesis.[24] For the first time, the NIR emission of lanthanide ions is realized by using 2D layered semiconductor material as the host. It has been proved that the introduction of lanthanide ions can expand the intrinsic narrow-band emission of layered TMDs. Compared with MoS_2 nanosheets, it has previously been reported that WSe_2 has more excellent optical properties.[25,26] Moreover, the doping engineering of p-type nature of WSe_2 rather than n-type of MoS_2 would broaden the application scope of optoelectronic devices based on 2D semiconductors. In addition, the phonon energy of the selenide semiconductor materials such as WSe_2 is lower than that of the sulfide semiconductor materials. The lower phonon energy of selenide hosts warrants a low probability for multi-phonon relaxations between the energy levels of lanthanide ions.[27] The upper energy levels can be readily non-radiatively quenched by multi-phonon transitions. Therefore, the radiative transition probabilities and luminescence of the lanthanide ions are improved due to the reduced multi-phonon relaxations. Recent report of our group suggested that monolayer InSe could be fabricated by pulsed laser deposition (PLD),[28] which presented excellent photoelectric properties. PLD is a classic physical bottom-up synthesis technique, and is generally utilized for the growth of oxide thin films. In recent years, PLD appears to be applicable for the deposition of 2D layered materials, such as MoS_2, WS_2 and *h*-BN, thanks to the advantages of the high growth rate, precise control of the thickness and stoichiometry transfer from target to thin film.[29,30] More importantly, 2D heterostructures could be *in situ* fabricated by PLD. In this work, we fabricated wafer-scale Yb^{3+}/Er^{3+} co-doped layered WSe_2 thin films by PLD. We take advantages of rare earth ions Yb/Er and apply them to the large scale 2D WSe_2 thin films. To improve the absorption of excitation energy and enhance the emission, Yb^{3+} ions have been co-doped as sensitizers due to their large absorption cross-section around 980 nm. The fast synthesis of Yb^{3+}/Er^{3+} co-doped WSe_2 layered thin films is demonstrated by PLD technique. In addition, the PL, crystallinity and continuity of the as-grown 2D layered WSe_2: Yb^{3+}/Er^{3+} thin films have also been studied by various techniques.

Experimental

The layered WSe_2:Yb/Er samples were deposited on SiO_2 (200 nm)/Si substrates by PLD with a polycrystalline target at 10 Hz laser frequency and 600 ^{o}C substrate temperature. Before the deposition, the chamber was evacuated to a base pressure of around 1×10^{-5} Pa. The bulk polycrystalline target was placed 4 cm in front of the substrates and ablated by a KrF pulsed laser (λ = 248 nm) with 320 mJ output energy. The thickness of the as-fabricated thin film can be controlled by the number of laser pulses, which permits the *in situ* specific modulation the number of WSe_2:Yb/Er layers. The polycrystalline target was prepared with composition $W_{0.985}Se_2$:$Yb_{0.01}Er_{0.005}$ (WSe_2:Yb/Er). Prior to the thin film preparation, a quartz tube containing the chemical elements demanded for the doped polycrystalline was evacuated to below 1×10^{-3} Pa and tightly sealed. Then the quartz tube was placed in a furnace for growing the polycrystalline at 600 °C for 24 h. The prepared WSe_2:Yb/Er target showed a prominent WSe_2 crystalline phase in the X-ray diffraction (XRD) pattern.

To identify crystal structure, X-ray diffractometer (Rigaku, SmartLab) with Cu Kα radiation (λ= 1.5406 Å) was used to record XRD patterns of the prepared films. The detailed microstructures and chemical compositions were measured by transmission electron microscope (TEM, JEOL JEM 2100F) equipped with an energy dispersive X-ray spectroscopy (EDX). The obtained samples were transferred onto copper grid for TEM characterization. A SKL-12 spectrometer modified with VG CLAM 4 multichannel hemispherical analyzer with a twin anode (Al/Mg) X-ray sources was used to perform XPS measurements. The base pressure for the measurement was 2×10^{-6} Pa. Raman spectra were recorded in a Horiba Jobin Yvon HR800 Raman microscopic system with a 488 nm laser. The PL spectra were measured using an Edinburgh FLSP920 spectrophotometer equipped with a commercial 980 nm laser diodes. All the measurements were carried out at room temperature.

Results and discussion

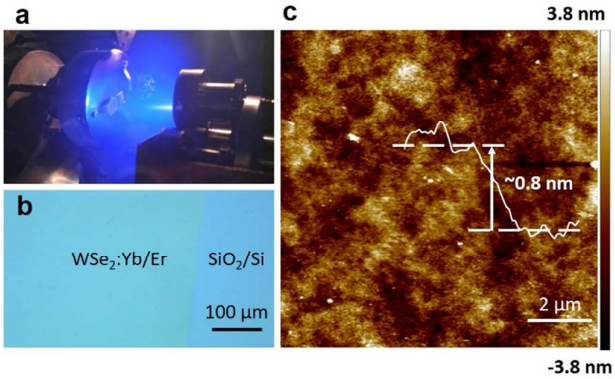

Fig. 1 Synthesis and images of WSe_2:Yb/Er. a, Schematic diagram of synthesis process for the WSe_2:Yb/Er thin films by laser ablation. b, Optical image of 1 cm×1 cm SiO_2/Si covered with WSe_2:Yb/Er thin film. c, AFM image of the WSe_2:Yb/Er thin film.

In this work, layered WSe_2:Yb/Er films were deposited on SiO_2/Si wafers by high-powered pulsed laser ablation. The surface of the polycrystalline WSe_2:Yb/Er target was stroked by

a focused high-powered pulsed laser beam in an ultra-high vacuum chamber, producing a plasma plume containing many energetic species including ions, atoms, molecules and clusters, which congregated thin film on the pre-heated wafer (Figure 1a). The as-grown thin films presented good continuity and uniformity across an area of approximate 1 cm^2 by the naked eye or under an optical microscope. Figure 1b presents an optical image of the prepared WSe_2:Yb/Er on a SiO_2/Si substrate deposited in 15 s with 10 Hz laser frequency. The as-prepared WSe_2:Yb/Er thin film is in light green color from optical microscopy. Moreover, the uniform morphology at the micrometer scale was investigated through atomic force microscopy (AFM) measurement. The typical AFM scanning images over 10 μm × 10 μm area is shown in Figure 1c. The average root-mean-square (RMS) roughness of WSe_2:Yb/Er thin films is 0.853 nm, indicating that the doping process has little effect on morphology of the WSe_2 films. The surface roughness values are similar with those of MoS_2 thin films prepared by PLD[31] and monolayer WS_2 prepared by chemical vapor deposition (CVD).[32] Due to the growth nature of PLD, the RMS roughness is strongly affected by some clusters generated by the high laser energy. The roughness can be further continuously optimized by adding a shadow mask or improving the quality of the substrate and target.[29] The height profile drawn at the edge suggests that the thickness of WSe_2:Yb/Er layers is ~0.8 nm, which is close to one atomic layer of WSe_2. The AFM results suggest that the prepared WSe_2:Yb/Er and WSe_2 thin films present a relatively flat surface.

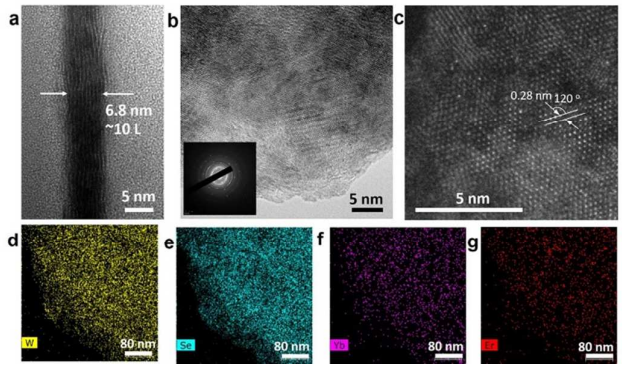

Fig. 2 TEM and CS-STEM images. a, The cross-sectional HR-TEM image of the WSe_2:Yb/Er samples deposited in 30 s with 10 Hz laser frequency. b, The in-plane HR-TEM with SAED and c, CS-STEM images of the WSe_2:Yb/Er samples deposited in 15 s with 10 Hz laser frequency. EDX analysis mapping images of W (d), Se (e), Yb (f), and Er (g) in the grown WSe_2:Yb/Er thin film.

The microstructures, layered structures, doping profile, and cross-sectional interface of the fabricated WSe_2:Yb/Er thin films are investigated by using high-resolution transmission electron microscopy (HR-TEM) and scanning transmission electron microscopy with EDX mapping. Figure 2a shows the cross-sectional HR-TEM image of the WSe_2:Yb/Er samples deposited in 30 s with 10 Hz laser frequency (300 pulses), revealing that the layered structure is preserved when Yb/Er is doped in WSe_2. 10 layered structure of 6.8 nm thick WSe_2:Yb/Er thin film is apparent. The growth rate can be estimated to be about 0.227 nm/s (1 layer/3 s at 10 Hz). Compared with the CVD method routinely used for growing 2D layers (~dozens of minutes), the growth speed by PLD is much faster.[29] From this image, the thickness of monolayer WSe_2:Yb/Er can be extracted to be 0.68 nm, which is similar with our AFM results and previous reports.[33] Moreover, the cross-sectional HR-TEM image suggests that monolayer WSe_2:Yb/Er can be deposited in 3 s with 10 Hz laser frequency. Figure 2b and 2c present the in-plane HR-TEM with the selected area electron diffraction (SAED) and spherical aberration corrected scanning transmission electron microscope (CS-STEM) images of the WSe_2:Yb/Er samples deposited in 15 s with 10 Hz laser frequency, indicating good crystalline quality of the hexagonal WSe_2 lattice. The lattice constant along (100) direction is 0.28 nm and the angle between (100) and (010) axes is 120°, which both agree with the previously reported atomic arrangement of WSe_2.[33] STEM-EDS mapping of elements (Figure 2d-g) show that the distributions of W, Se, Yb and Er elements are largely colocalized for WSe_2:Yb/Er samples, suggesting that rare earth ions Yb/Er have been homogeneously doped inside the as-prepared WSe_2:Yb/Er nanosheets. We have thus successfully developed layered WSe_2:Yb/Er thin films by PLD. The number of WSe_2:Yb/Er layers can be precisely controlled by adjusting the number of laser pulses.

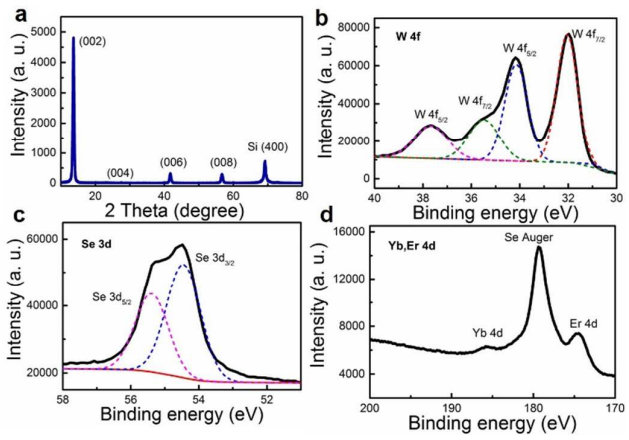

Fig. 3 XRD and XPS results. a, The XRD result of the PLD grown WSe_2:Yb/Er thin film. b, The fitted XPS spectra of W 4f core levels. c, The fitted XPS spectra of Se 3d core levels. d, The XPS spectra of Yb, Er 4d and Se Auger core levels.

The electrical and optical properties of the thin film are mainly determined by the crystal structure. Thus, it is important to investigate the crystallographic phase of the fabricated WSe_2:Yb/Er thin films. First, XRD was utilized to study the PLD grown thin films. According to the XRD result (Figure 3a), all peaks agree very well with the standard database (JCPDS card No. 38-1388), which can be assigned to

the (002) lattice orientations of hexagonal WSe_2. Doping concentrations of 1% Yb and 0.5% Er seem to have limited influence on the crystalline phase of hexagonal WSe_2. Moreover, the observation of only intense (00*l*) peaks specifies a highly textured WSe_2 nanosheet deposited on SiO_2/Si wafer with preferential orientation along c-axis. Figure 3b and 3c display the binding energy profiles for W 4f and Se 3d in the as-prepared samples, respectively. The separated peaks located at 32.05 and 34.15 eV are the footprints of the doublet W^{4+} $4f_{7/2}$ and W^{4+} $4f_{5/2}$ with spin-orbit split separation of 2.1 eV, while the peaks at 54.45 and 55.39 eV are assigned to the Se $3d_{5/2}$ and Se $3d_{5/2}$ binding energies with spin-orbit split separation of 0.94 eV. We have also observed the peaks at 35.48 and 37.66 eV that are assigned to W $4f_{5/2}$ and W $4f_{7/2}$, respectively, which could be attributed to potential oxidation reactions in air. All these results are in good agreement with earlier reports on WSe_2 thin films.[33] In addition, the distinct binding energy peaks corresponding to Er 4d core-level at 174.5 and Yb 4d core-level at 185.7 eV were detected in the WSe_2:Yb/Er samples (Figure 3d). The results match very well with the previously observed XPS features from $NaGdF_4$:Yb,Er nanoparticles.[34] The XRD and XPS results suggest that Yb/Er atoms are successfully incorporated into hexagonal WSe_2 lattice.

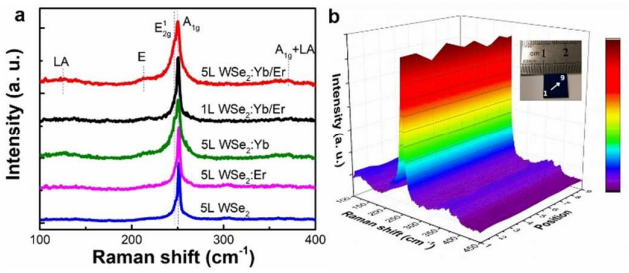

Fig. 4 Raman characterization. a, Raman spectra of the grown undoped and doped WSe_2 thin films, under 488 nm excitation. b, Raman spectra of nine spots in a line on the WSe_2:Yb/Er thin film surface.

Resonance Raman spectroscopy was utilized to evaluate the lattice vibration modes of few-layer WSe_2:Yb/Er thin films. The resonance Raman spectra is recorded when the incident laser energy is nearby the electronic transition energy of the sample, which can measure the electronic states in the materials because of electron-phonon interaction. In our work, we recorded the resonant transitions in both the undoped and lanthanide doped WSe_2 thin films with a 488 nm laser, respectively. Figure 4a shows the Raman spectra of the undoped and lanthanide doped WSe_2 thin films. Two distinctive peaks located at 246.4 cm^{-1} (attributed to the E^1_{2g} mode) and 250.3 cm^{-1} (originating from the A_{1g} mode) are recorded in 5 layered WSe_2:Yb/Er thin film. Some other weaker peaks as marked by the labels have also been identified, which can be assigned to second-order Raman modes. For monolayer WSe_2:Yb/Er, we only observed a single maximum around 250 cm^{-1}. As shown in Figure 4a, the Raman results of undoped and lanthanide (Yb, Er, Yb/Er) doped WSe_2 are in a good agreement with the previous reports,[35] indicating no significant changes to the Raman signature of WSe_2 because of the doping. The phonon energy of the WSe_2 is as low as 250 cm^{-1}, compared to 404 cm^{-1} of MoS_2. The lower phonon energy of WSe_2 matrix facilitates the reduction of the multi-phonon relaxations during the emission process, and therefore enhances the radiation transition from the dopant ions Yb^{3+}/Er^{3+} in principle. The previous reports suggest that coverage of the thin films, even the 2D materials, could be grown by PLD in a scalable and controllable way.[28-31] The inset of Figure 4b shows a photograph of the WSe_2:Yb/Er thin film with uniform appearance entirely covering the SiO_2/Si wafer with the in-plane dimension of 10 mm×10 mm. With the aim of confirming the uniformity of the thin film, we recorded the Raman spectroscopy of the selected nine spots in a line on the thin film as shown in the inset. All spots display the typical characteristic peaks of layered WSe_2 with similar profile and intensity, suggesting the homogeneous growth of WSe_2:Yb/Er thin films on the large scale up to centimetre size.

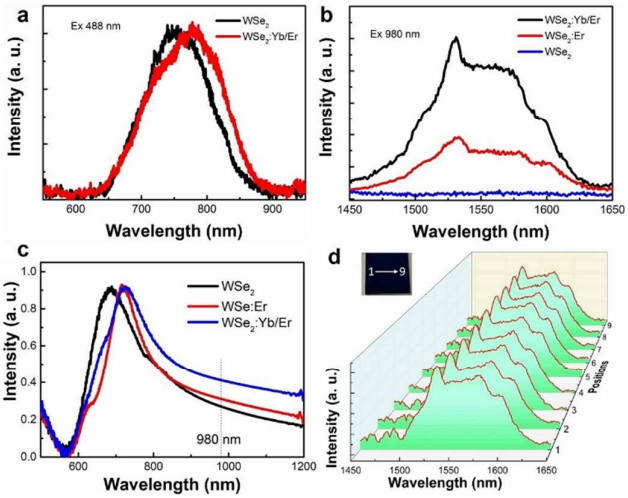

Fig. 5 PL and absorption spectra. a, The PL spectra of the prepared monolayer WSe_2 and WSe_2:Yb/Er samples under 488 nm excitation. b, The down-conversion emission spectra of the WSe_2, WSe_2:Er and WSe_2:Yb/Er thin films under 980 nm excitation. c, The refelected absorption spectra of WSe_2, WSe_2:Er and WSe_2:Yb/Er thin films. d, The NIR down-conversion emisison spectra of nine spots in a line on the WSe_2:Yb/Er thin film surface.

Followed by the structural, chemical and Raman spectra characterization, we have further measured the PL spectra of the prepared WSe_2:Yb/Er thin films. Figure 5a presents PL spectra of the prepared monolayer WSe_2 and WSe_2:Yb/Er samples under 488 nm excitation. The pristine monolayer WSe_2 generates an emission band around 750 nm. While the emission of monolayer WSe_2:Yb/Er shows a red shift, resulting in a more broad emission band at around 770 nm. The

prominent PL band from the monolayer sample accords with the direct A exciton reported in the range 1.4-1.8 eV (886-689 nm).[36] Compared with the monolayer sample, the few layers (bilayer, trilayer, etc.) present much weaker emission, which agrees well with the previous reports.[37] Under the excitation at 980 nm with a commercial diode laser, some interesting PL results have been found. As shown in Figure 5b, the down-conversion emissions have been observed at around ~1540 nm in both the WSe_2:Er and WSe_2:Yb/Er thin films, respectively. No such NIR down-conversion emission was observed in pristine WSe_2 samples under the identical test condition. The PL emission can be assigned to the emission transition of Er^{3+}, i.e. $^4I_{13/2}\rightarrow{}^4I_{15/2}$. Compared to the Er^{3+} singly doped WSe_2 sample, Yb/Er co-doped WSe_2 produces more efficient emission at around 1540 nm. The enhanced factor can reach up to 2.36. It is deduced that the improved NIR emission originates from the enhanced absorption cross section around 980 nm excitation due to the sensitization of Yb^{3+} ions. The mechanism of energy transition and transfer will be discussed later in this article. Figure 5c presents the diffuse reflected absorption spectra of the WSe_2, WSe_2:Er and WSe_2:Yb/Er thin films, respectively. The excitonic absorption peaks located at around 700 nm arises from direct gap transitions at the *K* point. The lanthanide ions doped WSe_2 samples show a red shift, differing from the undoped sample. Compared with WSe_2:Er, the absorption intensity of WSe_2:Yb/Er increases by the factor of 1.35 at around 980 nm, indicating that the introduction of Yb^{3+} ions can enhance the absorption at 980 nm. The pump power (*P*) dependence at 980 nm of the PL intensity (*I*) at 1540 nm has been recorded. The slope (*n*) of $I \propto P^n$ is 0.858 ± 0.015, confirming the down-conversion emission is a one-photon process, which is more efficient than the previously reported Er^{3+} singly doped MoS_2 films. In order to confirm the uniformity of the thin film and homogeneously distributions of Yb and Er elements, we measured the NIR emisison spectra from nine spots along one line on the thin films as shown in Figure 5d. The spot size is estimated to be approximately 0.5 mm^2. All spots show the typical characteristic peaks due to emission transition of Er^{3+} ($^4I_{13/2}\rightarrow{}^4I_{15/2}$) with similar profile and intensity, suggesting the homogeneous growth of WSe_2:Yb/Er thin films on the large scale up to centimeter size again.

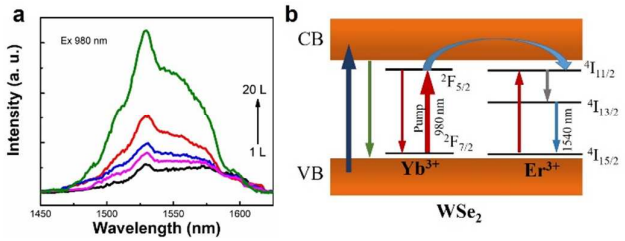

Fig. 6 NIR PL spectra and the energy levels diagram. a, The PL intensity of the different layered WSe_2:Yb/Er thin films under 980 nm excitation. b, The proposed energy band diagram and energy transfer mechanism in our synthesized WSe_2:Yb/Er thin film system.

As shown in Figure 6a, the PL intensity of WSe_2:Yb/Er thin films arises when the layered number increases, which could be explained by the fact that an increase in layer number leads to more gain from the luminescent ions. This phenomenon is different from the result in the emission from exciton in the layered 2D TMDs materials. Fortunately, even WSe_2:Yb/Er nanosheets become monolayer, the typical characteristic peak attributed to the emission transition of Er^{3+} ($^4I_{13/2}\rightarrow{}^4I_{15/2}$) doped into monolayer is still observable. Compared with the earlier result,[23] the NIR emission of Er^{3+} was only found in bilayer MoS_2. It is implied that both the enhanced optical absorption attributed to co-doping the sensitizer Yb^{3+} and the excellent optical properties of the host WSe_2 could lead to the observable NIR emission of Er^{3+} in monolayer TMDs nanosheets. Considering the energy levels of Yb^{3+}/Er^{3+}, the energy band diagram and energy transfer mechanism are illustrated in the synthesized WSe_2:Yb/Er system. Figure 6b shows the energy levels diagram of Yb^{3+}/Er^{3+} ions and the relevant energy transitions under 980 nm excitation. Firstly, the electrons of Yb^{3+} ions at $^2F_{7/2}$ are pumped to Yb^{3+}: $^2F_{5/2}$ states by the ground state absorption (GSA) under 980 nm photon pumping, in the meantime, the electrons of Er^{3+} ions at $^4I_{15/2}$ are pumped to Er^{3+}: $^4I_{11/2}$ state by GSA. Then the energy transfer (ET) takes place from the excited Yb^{3+} ions to the Er^{3+}: $^4I_{11/2}$ state. The Er^{3+} ions in $^4I_{11/2}$ level relax radiatively or nonradiatively to the lower $^4I_{13/2}$ level, then the Er^{3+} ions in $^4I_{13/2}$ level can be radiatively relaxed to the ground state Er^{3+}: $^4I_{15/2}$ and 1.54 μm emission occurs. It is well-known that low loss window around 1540 nm has been extensively utilized in optical communication and photonic technologies. Indeed, the ultimate goal of creating atomically ultrathin electronic and optoelectronic devices prompts the present concentrated studies on 2D layered materials. For that reason, the results as presented in Figure 5b and 5d suggest that Yb/Er co-doped WSe_2 not only produces considerably expanded luminescence of 2D TMDs to NIR telecommunication region beneficial to fundamental research, but also takes a novel chance to the progress of atomically thin NIR devices at 2D limit.

Conclusions

In summary, we have demonstrated fast fabrication of wafer-scale crystalline 2D WSe_2:Yb/Er layers by PLD. The growth rate can reach about 2.27 Å/s (1 layer/3 s at 10 Hz). The size of continuously high quality 2D WSe_2:Yb/Er thin films can be up to 1 cm^2. The deposition conditions could be precisely controlled to achieve the WSe_2:Yb/Er thin film with desired layer number. The crystal structure and chemical composition of the as-prepared thin films are studied, confirming that the grown thin film is highly textured WSe_2:Yb/Er nanosheets, and Yb/Er ions seem to have little effect on the stability of the layered WSe_2 crystal structure. High coherence and uniformity of few layered WSe_2:Yb/Er thin

films were confirmed by the Raman and PL spectra on different spots of the samples, respectively. More importantly, the luminescence of WSe_2 thin films simply excited by a single laser diode at 980 nm can be extended to telecommunication range at around 1540 nm, even the film is as thin as single atomic layer. The observed luminescence in monolayer WSe_2:Yb/Er is ascribed to both the excellent photonic properties of WSe_2 host and co-doping Yb^{3+} sensitizer. Our work indicates that the PLD grown lanthanide ions doped TMDs this films not only exhibit wafer scale and good crystalline, but also show excellent optical properties. The developed layered WSe_2:Yb/Er thin films in this work are promising for atomically thin NIR photonic devices in 2D limit, and also show potential to be a platform for fast fabricating van der Waals heterostructures based on doped TMDs by PLD.

Conflicts of interest

There are no conflicts to declare.

Acknowledgements

The research was supported by the grants from the Research Grants Council (RGC) of Hong Kong (RGC GRF No. PolyU 153281/16P).

Notes and references

1 S. Han, X. Qin, Z. An, Y. Zhu, L. Liang, Y. Han, W. Huang, X. Liu, *Nat. Commun.* 2016, **7**, 13059.
2 M.-K. Tsang, G. X. Bai, J. H. Hao, *Chem. Soc. Rev*. 2015, **44**, 1585-1607.
3 H. Dong, L. D. Sun, C. H. Yan, *Chem. Soc. Rev.* 2015, **44**, 1608-1634.
4 G. X. Bai, M.-K. Tsang, J. H. Hao, *Adv. Funct. Mater.* 2016, **26**, 6330-6350.
5 J. C. G. Bunzli, S. V. Eliseeva, *Chem. Sci*. 2013, **4**, 1939-1949.
6 J. Zhou, Q. Liu, W. Feng, Y. Sun, F. Li, *Chem. Rev.* 2015, **115**, 395-465.
7 B. Liu, C. Li, P. Yang, Z. Hou, J. Lin, *Adv. Mater.* 2017, **29**, 1605434.
8 T. N. Theis, P. M. Solomon, *Science* 2010, **327**, 1600-1601.
9 M. Lundstrom, *Science* 2003, **299**, 210-211.
10 S. B. Desai, S. R. Madhvapathy, A. B. Sachid, J. P. Llinas, Q. Wang, G. H. Ahn, G. Pitner, M. J. Kim, J. Bokor, C. Hu, *Science* 2016, **354**, 99-102.
11 B. Liu, C. Li, G. Chen, B. Liu, X. Deng, Y. Wei, J. Xia, B. Xing, P. A. Ma, J. Lin, *Adv. Sci.* 2017, **4**, 1600540.
12 X. Duan, C. Wang, J. Shaw, R. Cheng, Y. Chen, H. Li, X. Wu, Y. Tang, Q. Zhang, A. Pan, J. Jiang, R. Yu, Y. Huang, X. Duan, *Nat. Nanotechnol.* 2014, **9**, 1024.
13 Z. Yin , H. Li , H. Li , L. Jiang , Y. Shi , Y. Sun , G. Lu , Q. Zhang , X. Chen, H. Zhang, *ACS Nano* 2012, **6**, 74.
14 C. L. Tan, Z. C. Lai, H. Zhang, *Adv. Mater*. 2017, 1701392.
15 W. Xu, W. Liu, J. F. Schmidt, W. Zhao, X. Lu, T. Raab, C. Diederichs, W. Gao, D. V. Seletskiy, Q. Xiong, *Nature* 2017, **541**, 62-67.
16 C. Tan, X. Cao, X. J. Wu, Q. He, J. Yang, X. Zhang, J. Chen, W. Zhao, S. Han, G. H. Nam, M. Sindoro, H. Zhang, *Chem. Rev*. 2017, **117**, 6225-6331.
17 Y. Liu, N. O. Weiss, X. Duan, H.-C. Cheng, Y. Huang, X. Duan, *Nat. Rev. Mater*. 2016, **1**, 16042.
18 V. P. Pham, G. Y. Yeom, *Adv. Mater.* 2016, **28**, 9024-9059.
19 Z. Li, J. Zheng, Y. Zhang, C. Zheng, W. Y. Woon, M. C. Chuang, H. C. Tsai, C. H. Chen, A. Davis, Z. Q. Xu, J. Lin, H. Zhang, Q. Bao, *ACS Appl. Mater. Interfaces* 2017, **9**, 34204-34212.
20 J. Gao, Y. D. Kim, L. Liang, J. C. Idrobo, P. Chow, J. Tan, B. Li, L. Li, B. G. Sumpter, T. M. Lu, V. Meunier, J. Hone, N. Koratkar, *Adv. Mater*. 2016, **28**, 9735-9743.
21 K. Zhang, S. Feng, J. Wang, A. Azcatl, N. Lu, R. Addou, N. Wang, C. Zhou, J. Lerach, V. Bojan, M. J. Kim, L. Q. Chen, R. M. Wallace, M. Terrones, J. Zhu, J. A. Robinson, *Nano Lett.* 2015, **15**, 6586-6591.
22 W. J. Jie, Z. B. Yang, F. Zhang, G. X. Bai, C. W. Leung, and J. H. Hao, *ACS Nano* 2017, **11**, 6950.
23 Y. Shi, H. Li, L.-J. Li, *Chem. Soc. Rev.* 2015, **44**, 2744-2756.
24 G. X. Bai, S. G. Yuan, Y. D. Zhao, Z. B. Yang, S. Y. Choi, Y. Chai, S. F. Yu, S. P. Lau, J. H. Hao, *Adv. Mater.* 2016, **28**, 7472-7477.
25 J. S. Ross, P. Klement, A. M. Jones, N. J. Ghimire, J. Yan, D. G. Mandrus, T. Taniguchi, K. Watanabe, K. Kitamura, W. Yao, D. H. Cobden, X. Xu, *Nat. Nanotechnol.* 2014, **9**, 268-272.
26 K. L. Seyler, J. R. Schaibley, P. Gong, P. Rivera, A. M. Jones, S. Wu, J. Yan, D. G. Mandrus, W. Yao, X. Xu, *Nat. Nanotechnol.* 2015, **10**, 407-411.
27 S. Zhang, P. Němec, V. Nazabal, Y. Jin, *Optoelectron. Lett.* 2016, **12**, 199-202.
28 Z. B. Yang, W. J. Jie, C.-H. Mak, S. H. Lin, H. H. Lin, X. F. Yang, F. Yan, S. P. Lau, and J. H. Hao, *ACS Nano* 2017, **11**, 4225.
29 Z. B. Yang, J. H. Hao, *J. Mater. Chem. C* 2016, **4**, 8859.
30 M. I. Serna, S. H. Yoo, S. Moreno, Y. Xi, J. P. Oviedo, H. Choi, H. N. Alshareef, M. J. Kim, M. Minary-Jolandan, M. A. Quevedo-Lopez, *ACS Nano* 2016, **10**, 6054-6061.
31 F. Ullah, V. Senthilkumar, S. H. Kim, C. T. Le, H. Rock, D. Y. Lee, S. Park, A. I. Ali, Y. S. Kim, *J. Nanosci. Nanotechnol.* 2016, **16**, 10284-10289.
32 C. Ma, Y. Shi, W. Hu, M. H. Chiu, Z. Liu, A. Bera, F. Li, H. Wang, L. J. Li, T. Wu, *Adv. Mater.* 2016, **28**, 3683-3689.
33 J.-K. Huang, J. Pu, C.-L. Hsu, M.-H. Chiu, Z.-Y. Juang, Y.-H. Chang, W.-H. Chang, Y. Iwasa, T. Takenobu, L.-J. Li, *ACS Nano* 2013, **8**, 923-930.
34 P. Ramasamy, P. Chandra, S. W. Rhee, J. Kim, *Nanoscale* 2013, **5**, 8711-8717.
35 S.-Y. Chen, C. Zheng, M. S. Fuhrer, J. Yan, *Nano Lett.* 2015, **15**, 2526-2532.
36 M. P. Deshpande, G. K. Solanki, and M. K. Agarwal, *Mater. Lett*. 2000, **43**, 66-72.
37 P. Tonndorf, R. Schmidt, P. Böttger, X. Zhang, J. Börner, A. Liebig, M. Albrecht, C. Kloc, O. Gordan, D. R. Zahn, *Opt. Express* 2013, **21**, 4908-4916.